TELLUS

Comparison of the radiative properties and direct radiative effect of aerosols from a global aerosol model and remote sensing data over ocean

By GUNNAR MYHRE[1,2,3]*, NICOLAS BELLOUIN[4], TORE F. BERGLEN[1], TERJE K. BERNTSEN[1,2], OLIVIER BOUCHER[4], ALF GRINI[1,5], IVAR S. A. ISAKSEN[1], MONA JOHNSRUD[3], MICHAEL I. MISHCHENKO[6], FRODE STORDAL[1,3] and DIDIER TANRÉ[7],
[1]*Department of Geosciences, University of Oslo, PO Box 1022, Blindern, 0315 Oslo, Norway;* [2]*Center for International Climate and Environmental Research – Oslo, Norway;* [3]*Norwegian Institute for Air Research, Norway;* [4]*Met Office, Exeter, UK;* [5]*Meteo-France (CNRM/GMEI), France;* [6]*NASA Goddard Institute for Space Studies, New York, USA;* [7]*Laboratoire d'Optique Atmosphérique, Centre National de la Recherche Scientifique, Université des Sciences et Technologies de Lille,Villeneuve d'Ascq, France*

ABSTRACT

A global aerosol transport model (Oslo CTM2) with main aerosol components included is compared to five satellite retrievals of aerosol optical depth (AOD) and one data set of the satellite-derived radiative effect of aerosols. The model is driven with meteorological data for the period November 1996 to June 1997 which is the time period investigated in this study. The modelled AOD is within the range of the AOD from the various satellite retrievals over oceanic regions. The direct radiative effect of the aerosols as well as the atmospheric absorption by aerosols are in both cases found to be of the order of 20 Wm^{-2} in certain regions in both the satellite-derived and the modelled estimates as a mean over the period studied. Satellite and model data exhibit similar patterns of aerosol optical depth, radiative effect of aerosols, and atmospheric absorption of the aerosols. Recently published results show that global aerosol models have a tendency to underestimate the magnitude of the clear-sky direct radiative effect of aerosols over ocean compared to satellite-derived estimates. However, this is only to a small extent the case with the Oslo CTM2. The global mean direct radiative effect of aerosols over ocean is modelled with the Oslo CTM2 to be –5.5 Wm^{-2} and the atmospheric aerosol absorption 1.5 Wm^{-2}.

1. Introduction

Global aerosol modelling has reached the point where validations against measurements and satellite data have become a necessary and important step to improve estimates of radiative forcing due to aerosols. The global aerosol models are important tools for estimating the anthropogenic fraction of the current aerosol content as well as future predictions of the atmospheric aerosol loading. The uncertainties in the climate effect of aerosols arise from such a wide range of causes that a multitechnique approach is needed (Haywood and Boucher, 2000; Houghton, 2001; Ramanathan et al., 2001; Kaufman et al., 2002). An increasing number of aerosol measurements have be-

come available over the last years. These include surface in situ measurements, ground-based column aerosol observations, aircraft measurements, and satellite data. Multicomponent global aerosol models have recently become available. They are essential for interpretation of column measurements. On the other hand, the column measurements are important in validation of the models. Significant attention has been given to absorbing aerosols with regard to the direct aerosol effect (Haywood and Shine, 1995; Sato et al., 2003), the semidirect aerosol effect (Ackerman et al., 2000; Hansen et al., 1997), as well as global warming and local cooling induced by these aerosols (Menon et al., 2002). Due to the importance of the absorbing aerosol methods to validate their distribution in global models are vital. Anthropogenic as well as natural aerosols need to be taken into account.

Satellite retrievals have provided useful knowledge into the field of climate effects of aerosols (Kaufman and Fraser, 1997;

Haywood et al., 1999; Wetzel and Stowe, 1999; Ackerman et al., 2000; Kuang and Yung, 2000; Nakajima et al., 2001; Tanré et al., 2001; Rosenfeld et al., 2002; Sekiguchi et al., 2003; Bellouin et al., 2005; Kaufman et al., 2005). Several aerosol retrievals from various instruments and satellite platforms have provided much information on aerosol optical depth (Husar et al., 1997; Stowe et al., 1997; Nakajima and Higurashi, 1998; Torres et al., 1998; Goloub et al., 1999; Mishchenko et al., 1999; Kahn et al., 2005; Remer et al., 2005). Abdou et al. (2005), Myhre et al. (2005) and Myhre et al. (2004a) compared various aerosol satellite retrievals and found significant differences, but also regions and time periods with promising similarities. For improved knowledge of the direct aerosol effect, it is of particular value that several recent studies have provided the radiative effect of aerosols from remote sensed data (Boucher and Tanré, 2000; Christopher and Zhang, 2002; Loeb and Kato, 2002; Bellouin et al., 2003; Zhang et al., 2005). Yu et al. (2006) summarized 11 estimates of the clear-sky aerosol direct radiative effect at the top of the atmosphere based on remote sensed data, finding a range from -7.1 to -3.8 Wm^{-2} and a mean of -5.5 Wm^{-2}. Fewer estimates of the absorption by the aerosols in the atmosphere were available but the mean of 7 estimates was 3.3 Wm^{-2}. Generally, the estimates of the radiative effect of aerosols (at the top of the atmosphere and at the surface) from the five available models were substantially weaker than the estimates based on remote sensed data (Yu et al., 2006).

In this study, a global aerosol transport model (Oslo CTM2) is used to estimate the aerosol optical depth (AOD) and the radiative effect of aerosols over ocean. The model has been validated against ground measurements in Grini et al. (2002), Grini et al. (2005) and Berglen et al. (2004), and against aircraft measurements in Myhre et al. (2003a) and Myhre et al. (2003b) for various aerosol types. The main aerosol components, mineral dust, sea salt, sulphate, organic carbon and black carbon, are included in the model. In this work, stratospheric aerosols are neglected (Myhre et al., 2004b). We restrict this study to comparison with column information mainly from satellite retrievals, but we also use measurements from sunphotometers. The time period from November 1996 to June 1997 is chosen here as AODs from five different satellite retrievals in this period have already been compared and converted to a common format (Myhre et al., 2004a). Furthermore, an advantage with the period chosen is that the radiative effect of aerosols derived from one of these five satellite data sets, the POLDER instrument, is well documented in the literature (Boucher and Tanré, 2000; Bellouin et al., 2003). The results from the aerosol model will be compared with the satellite-retrieved data. The aim of this study is not to perform a judgement of the available observational data, rather an evaluation of the global aerosol model against information available for the time period of investigation is performed.

2. The global aerosol model

2.1. General description of the transport model

Oslo CTM2 is an offline chemical transport/tracer model (CTM) that uses pre-calculated meteorological fields to simulate tracer distributions in the atmosphere. The model has been used in a wide range of studies of the change in atmospheric chemical composition (Gauss et al., 2003a; Gauss et al., 2003b; Isaksen et al., 2005) and for atmospheric aerosols (Grini et al., 2002; Myhre et al., 2003a; Myhre et al., 2003b; Berglen et al., 2004; Myhre et al., 2004b; Grini et al., 2005). The spatial resolution of the model depends on the input of meteorological data. In this study, forecast data from European Centre for Medium-Range Weather Forecasts (ECMWF) have been used. The meteorological input data have been generated by running the Integrated Forecast System (IFS) model at ECMWF in a series of forecasts starting from the analysed fields every 24 h. Each forecast is run for 36 h, allowing for 12 h of spin-up and the last 24 h are diagnosed every third hour, generating a continuous record of input data. This produces standard ECMWF model output (cloud cover, surface properties etc.) and in addition a consistent data set with other relevant data (boundary layer height, convection, and three-dimensional rainfall) used in the CTM. The use of the IFS model allows a higher temporal resolution of 3 h compared to the standard of 6 h for archived data, and thus a more consistent data set. For this study, the meteorological data for 1996 are in T63 resolution (1.875° × 1.875°) with 19 layers and the data for 1997 are in T42 (2.825° × 2.825°) with 40 layers. This difference in model resolution has small impact on the aerosol load.

The advection of chemical species is calculated by the second-order moment method, which is able to maintain large gradients in the distribution of species (Prather, 1986). Vertical mixing by convection is based on the surplus and deficit of mass flux in a column (Tiedtke, 1989). Turbulent mixing in the boundary layer is treated according to the Holtslag K-profile scheme (Holtslag et al., 1990).

Dry deposition includes both uptake on the ground and turbulent mix-out for all species. Gravitational settling is included for sea salt and mineral dust. Wet deposition is treated separately for large-scale and convective precipitation, since the convective precipitation is coupled directly to the vertical transport (Berglen et al., 2004). The atmospheric loss terms are described in more detail in the respective aerosol-type sections below.

2.2. Sea salt

Sea salt is simulated using the formulation of Grini et al. (2002). The source formulation of Monahan et al. (1986) is used for small particles and the source formulation of Smith et al. (1993) is used for larger particles. The aerosols are allowed to grow

Table 1. Emissions and aerosol optical depth of the aerosol components included in the model for the period November 1996 to June 1997

	Emission (Tg/month)			Aerosol optical depth
Sulphate	SO_2		7.49	0.039
	SO_4		0.22	
	DMS		0.95	
Black carbon FF		0.42		0.0011
Organic carbon FF		1.88		0.0047
Biomass burning	BC		0.50	0.025
	OC		3.11	
Mineral dust		133		0.024
Sea salt		731		0.055

The emission of sulphuric species is given as Tg(S)/month, whereas for organic carbon as Tg(C)/month. The sea salt emissions are dry aerosols.

to their equilibrium size with the ambient relative humidity (Fitzgerald, 1975), and they are removed from the atmosphere by dry deposition (Seinfeld and Pandis, 1998) and wet deposition. Large-scale and convective wet deposition are calculated separately as in (Berglen et al., 2004). Eight bins are used to transport seasalt. The bins are logarithmically evenly distributed with the smallest dry diameter being 0.03 μm and the largest dry diameter being 25 μm. The lifetime decreases with size since dry deposition is more efficient for the largest sizes. The global emissions of the various aerosol components are shown in Table 1.

2.3. Mineral dust

Mineral dust is simulated using the Dust Entrainment and Deposition model of Zender et al. (2003). The source formulation uses subgrid wind speed variability from Justus et al. (1978) so that dust can be mobilized even though the mean wind speed does not exceed the threshold wind for mobilization. The emissions are weighted by an erodibility factor accounting for that some deserts are more erodible than others (Ginoux et al., 2001). The erodibility factor in Oslo CTM2 is based on the idea that reflective areas can be more erodible than other areas (Grini et al., 2005). Most of the dust mass is emitted with a mode having a mass median diameter of 4.82 μm. In the current simulations, eight bins are used to transport mineral dust. The bins are logarithmically evenly distributed with the smallest dry diameter being 0.06 μm and the largest being 50 μm.

2.4. Sulphate

Five sulphur components have been included in the Oslo CTM2; DMS, SO_2, sulphate, H_2S and MSA (Berglen et al., 2004). In terms of emissions, anthropogenic emissions of SO_2 and subse-

quent oxidation to sulphate constitute the most important source in the sulphur cycle, although natural emissions of DMS and volcanic emissions of SO_2 are important in remote areas. Oxidation of SO_2 to sulphate takes place both in the aqueous phase (by O_3, H_2O_2, HO_2NO_2 and metals) and in the gas phase by OH. Oxidation by OH contributes to formation of new aerosols, whereas aqueous phase oxidation occurs on pre-existing particles. Aqueous phase oxidation rates are determined using meteorological cloud data, Henry's law constants and chemical equilibrium constants and rates are included in the QSSA chemical solver used in the model. This method permits online calculation of the aqueous phase chemistry. Atmospheric sulphur is eventually lost by deposition, mainly by dry deposition of SO_2 or by wet deposition of sulphate.

2.5. Carbonaceous particles

Carbonaceous aerosols are implemented following Cooke et al. (1999). Both BC and OC are separated into a hydrophobic fraction and a hydrophilic fraction. Emissions of BC are assumed to be 80% hydrophobic, while for OC this figure is 50% (Cooke et al., 1999). Hydrophobic aerosols are aged (oxidized or coated by a hydrophilic compound) in the atmosphere and then become hydrophilic with an exponential lifetime of 1.15 days. Dry deposition of hydrophilic carbonaceous aerosols is calculated with a deposition velocity of 0.025 cm s^{-1} over dry surfaces (land) and 0.2 cm s^{-1} over oceans. For hydrophobic aerosols, a deposition velocity of 0.025 cm s^{-1} is applied for all surfaces. The hydrophilic aerosols are also removed by wet deposition. They are assumed to be totally absorbed in the cloud droplets, and are removed according to the fraction of the liquid water content (LWC) of a cloud that is removed by precipitation, as described in Berglen et al. (2004).

2.6. Aerosol optical properties

The optical properties are calculated for six different aerosol types, namely sea salt, mineral dust, sulphate, and carbonaceous particles which are divided into three components; fossil fuel (FF) black carbon, organic carbon and biomass burning aerosols (see Table 2). For mineral dust and sea salt size distributions are calculated in the transport model, and are used in Mie theory calculations of the optical properties. For sulphate, organic and black carbon pre-defined dry lognormal size distributions are adopted in the Mie calculations of optical properties. The size distributions, refractive indices (at 550 nm), and assumptions regarding hygroscopic growth of the various aerosols are shown in Table 2.

Internal mixture of BC and OC is included for the biomass burning aerosols (Myhre et al., 2003a). For the rest of the aerosol components, external mixing is assumed. The refractive indices for sea salt, sulphate, and black carbon are taken from the standard literature. For mineral dust and aerosols from biomass

Table 2. Information of size distribution, refractive indices, and hygroscopic growth for the aerosol components in the Oslo CTM2

	Mineral dust	Sea salt	Sulphate	Black carbon	Organic carbon	Biomass burning[a]
Size distribution	Modelled	Modelled	$R_m = 0.05$, $\sigma = 2.0$	$R_m = 0.0118$, $\sigma = 2.0$	$R_m = 0.05$, $\sigma = 2.0$	Three modes[a]
Refractive indices at 550 nm (r-real, im-imaginary)	r:1.475, im:0.00126[b]	r:1.5, im:1.e-8 (Shettle and Fenn, 1979)	r: 1.529 im:1.e-7 (Toon et al., 1976)	r:1.75, im:0.44 (WCP, 1986)	r: 1.529 im:1.0e-7 Similar to sulphate	r:1.54 im:0.018[a]
Hygroscopic growth	No	(Fitzgerald, 1975)	(Fitzgerald, 1975)	No	(Peng et al., 2001)	No

R_m is the geometric mean number radius (in μm) and σ is the geometric standard deviation in the lognormal size distribution.
[a]Based on SAFARI-2000 results, see further details in Haywood et al. (2003a) and Myhre et al. (2003a).
[b]Based on the SHADE campaign, see further details in Myhre et al. (2003b).

burning information from the aerosol campaigns SHADE and SAFRAI-2000 is used, respectively. Fossil fuel organic carbon is assumed to be purely scattering with similar refractive indices as for sulphate aerosols. This is justified by the study of (Myhre and Nielsen, 2004) who investigated a class of water soluble organic acids, with negligible absorption. Jacobson (1999), however, found that the absorption could be significant in the UV and visible region for certain organic compounds. A more detailed understanding of the organic compounds is needed in order to improve their optical properties.

Hygroscopic growth is included for sea salt, sulphate, and the hydroscopic fraction of organic carbon. Water uptake is included up to 99.5% relative humidity. Parametrization of the water uptake is based on the study of Fitzgerald (1975) for sulphate and sea salt and Peng et al. (2001) for OC. For sulphate the parametrization of Fitzgerald was tested against solving the Kohler equation, with almost identical results (Myhre et al., 2004c). In Myhre et al. (2004c), it was found that subgrid variation in relative humidity could significantly strengthen the radiative effect of sulphate aerosols. Further it was found that different data sets of relative humidity could result in significantly different water uptake for sulphate aerosols. In this work, the ECMWF IFS relative humidity data are used with no subgrid variability. Based on the SAFARI-2000 measurements, an increase of 20% of biomass burning aerosol mass due to non-carbonaceous material (Formenti et al., 2003) is included.

Mineral dust and sea salt particles may be non-spherical, but it is shown in Mishchenko et al., (1995) that for radiative fluxes Mie theory (assuming spherical particles) is reasonable.

2.7. Radiative transfer calculations

A multistream model using the discrete ordinate method (Stamnes et al., 1988) is adopted for the radiative transfer calculations in the solar spectrum. The model includes gas absorption, Rayleigh scattering, absorption and scattering by aerosols, and scattering by clouds. In the current simulations, eight streams are used with four spectral regions, see further details in Myhre et al. (2002). The radiative transfer calculations are performed offline so the aerosols do not feed back on to the meteorology.

3. Remote sensing data

The global aerosol model is compared against remote sensing techniques for information of column aerosol characteristics, mainly the aerosol optical depth (AOD). Various satellite retrievals and ground-based sun-photometers from the AERONET network will be used to evaluate whether the global aerosol model gives reasonable results for the time period studied. An important part of this study is comparison between the global aerosol model and satellite-derived direct radiative effect of aerosols and absorption of aerosols in the atmosphere.

3.1. Satellite data

In the period November 1996 to June 1997, five satellite retrievals of AOD over global ocean are available. In this period, the POLDER and OCTS instruments were operating onboard the ADEOS satellite platform. In addition, aerosol retrievals from the long term AVHRR and TOMS 2 instruments were available. For AVHRR actually two retrievals were accessible; namely one-channel and two-channel retrievals. These altogether five aerosol satellite retrievals are compared for monthly mean data on a common format in Myhre et al. (2004a). A description of the algorithms used in the aerosol retrievals can be found in Myhre et al. (2004a) and references therein.

3.2. AERONET

AERONET is a world wide network of ground-based sun-photometers (Holben et al., 1998). The main information from AERONET is spectral AOD, but information such as size distribution, single scattering, and refractive indices can also be retrieved. Monthly mean Level 2 AOD data are adopted and this is the same as used in Myhre et al. (2004a).

3.3. Radiative effect of aerosols and absorption by the aerosols derived from POLDER

In the POLDER aerosol retrieval, 12 different models are used. These consist of four values for the modal radius and three values for the refractive index. Based on the selection of the aerosol model along with single scattering albedo values from the AERONET offline radiative transfer calculations have been performed (Bellouin et al., 2003; Boucher and Tanré, 2000). Calculations of the radiative effect of aerosols at the top of the atmosphere and at the surface are performed. From this the absorption in the atmosphere by aerosols are derived (Bellouin et al., 2003). In Bellouin et al. (2003), sea salt aerosols are assumed to have a single scattering albedo of 0.98. In this study, the radiative effects of aerosols from POLDER have been recomputed assuming purely scattering sea salt aerosols. We use this new data set except where stated otherwise.

4. Results

4.1. Model results

Figure 1 shows the global distribution of AOD at 550 nm for sulphate aerosols, fossil fuel black carbon, fossil fuel organic carbon, sea salt, mineral dust, and biomass burning aerosols for the period November 1996 to June 1997. The spatial patterns of the different aerosol species are quite dissimilar. The black carbon and organic carbon from fossil fuel burning have the most similar pattern. Sulphate aerosols have also highest AOD in industrial regions, but sulphate has significant AOD over ocean as
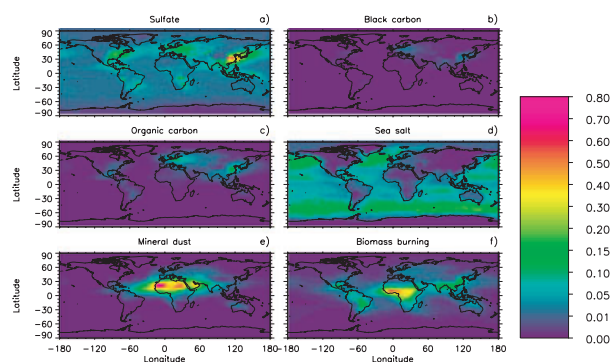

Fig. 1. Aerosol optical depth at 550 nm from Oslo CTM2 in the period November 1996 to June 1997 for various aerosol components (a) sulphate, (b) black carbon, (c) organic carbon, (d) sea salt, (e) mineral dust, and (f) biomass burning.

well. Sea salt AOD is very low over land, whereas over ocean it is as high as 0.2 around 50° latitude in both hemispheres, where surface wind is large. The highest AOD is from mineral dust with particularly high values over the Saharan and Arabian deserts. Over the Atlantic Ocean, the transport of Saharan dust is clearly evident. For the period investigated here, the highest AOD from biomass burning aerosol is in the African sub-Sahelian region, but transport over the Atlantic Ocean is significant. The AOD for the aerosols from biomass burning over the Atlantic Ocean is somewhat weaker and generally displaced somewhat southward compared to mineral dust AOD. South East Asia and southern America are also regions with biomass burning aerosols. However, the main biomass burning season during July to September in southern America as well as in southern Africa is not included in the time period considered here. The aerosol components with a source over land are clearly transported over ocean, in particular in coastal regions. However, over remote oceanic regions sea salt aerosols and sulphate aerosols are clearly dominating. The global mean AOD is shown in Table 1, with sea salt having the highest global mean AOD in these model simulations.

4.2. Comparison of model and satellite-retrieved AOD

Aerosol optical depth from five different satellite retrievals and based on the Oslo CTM2 are shown in Fig. 2. There are many striking features that agree between the model and the satellite retrievals, but there are also significant differences. The highest AOD is found off the west coast of Africa and from Fig. 1 it can be seen to be due to mineral dust and biomass burning aerosols. Further the model reproduces the general pattern of the satellite retrieval results with higher AOD in coastal areas compared to remote oceanic regions. In Myhre et al. (2004a), it was found that the largest difference between the satellite retrievals was in the Southern Hemisphere around 50°. The modelled AOD in this region lies within the range of the satellite retrievals.
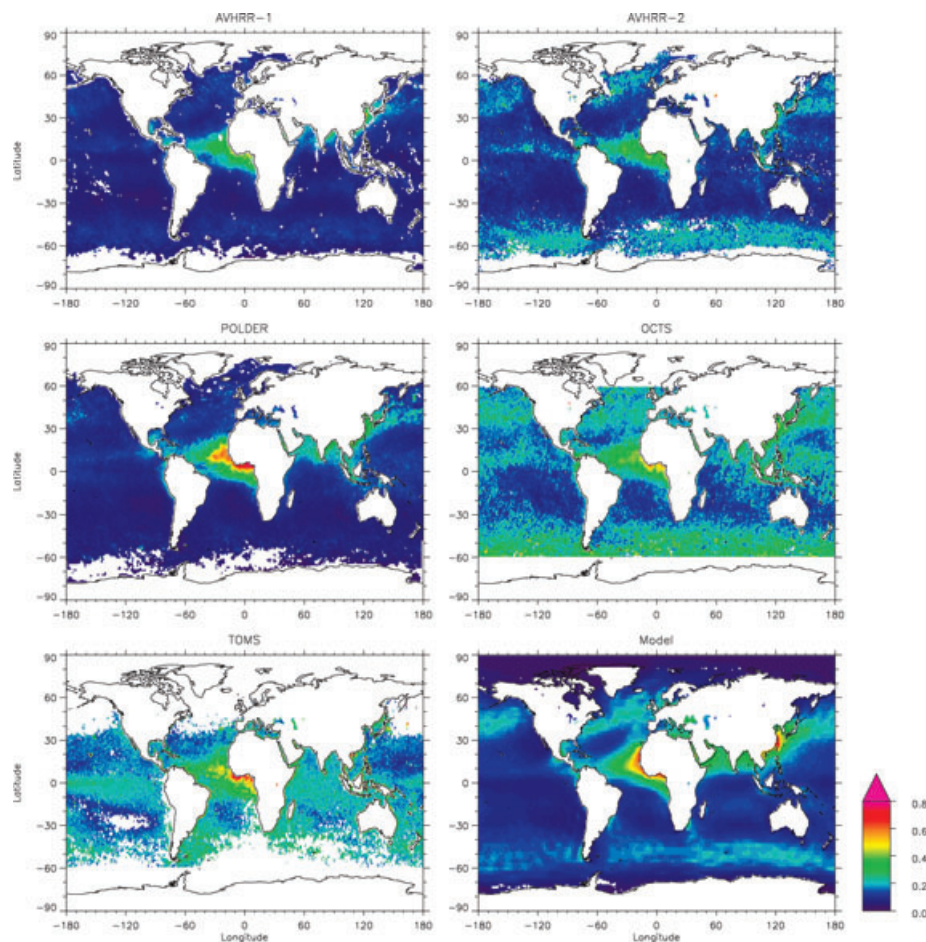
Fig. 2. Averaged AOD (550nm) over ocean for the period Nov 96-Jun 97. Maximum AOD is 0.77, 1.00, 1.21, 1.35, 1.80 and 0.72, respectively, for AVHRR-1, AVHRR-2, POLDER, OCTS, TOMS and Model. Values are given with minimum of data for two months.

At high latitudes, the model seems to have values closest to the AVHRR-2 retrievals. Off the coast of the Saharan desert, the values seem closest to the POLDER satellite retrieval. Non-spherical particles and aerosol retrievals of these may be one possible cause of difference between the model and the satellite aerosol retrievals (Mishchenko et al., 2003). However, several causes can here contribute to the differences.

The zonal mean of the AOD shown in Fig. 3a illustrates that the model is within the range of the satellite retrievals. The model AOD follows variations similar to those of the satellite retrievals with highest values around 50°S, 10°N, and 40°N. Figure 3b shows the temporal variation in the global mean AOD and as in Fig. 3a the model has values closest to the AVHRR-2 satellite retrieval. Note the nice similarity in pattern in the seasonal variation for the model and all the satellite retrievals.

Similar to Myhre et al. (2004a), we emphasize the coastal areas with elevated AOD compared to most of the remote oceanic regions. Aerosols in coastal regions have often a more complex chemical composition than those in remote oceanic regions, see Fig. 1. Based on the analysis in Fig. 2 and from Myhre et al. (2004a), many of the 11 coastal regions shown in Fig. 4 the agreement between the satellite-retrieved AOD is better than in most remote oceanic regions. In most coastal regions the model AOD is within the range of the satellite retrievals. The largest differences between the model and the satellite retrievals are seen for a few months over the Cape Verde Plateau, the Arabian Sea, and the Red Sea. These are regions with relatively high AOD and some satellite retrievals have upper threshold values for AOD to distinguish between aerosol and clouds. Indeed, for very high AOD, such as large dust outbreaks, most satellite retrievals have problems to retrieve aerosol information (Myhre et al., 2005). The seasonal variation of AOD in the model follows the satellite data quite nicely. In the oceanic regions downwind to the main areas with industrial pollution in the Northern Hemisphere, there is a clear increase in AOD from the winter to the summer, except in the South China Sea.

Fig. 3. Zonal mean AOD for the six data sets at 550 nm (eight month means). Global, Southern Hemisphere, and Northern Hemisphere mean AODs over ocean (monthly means).
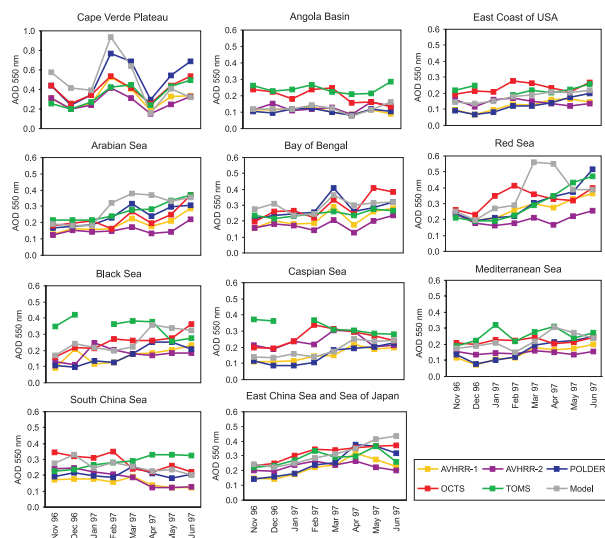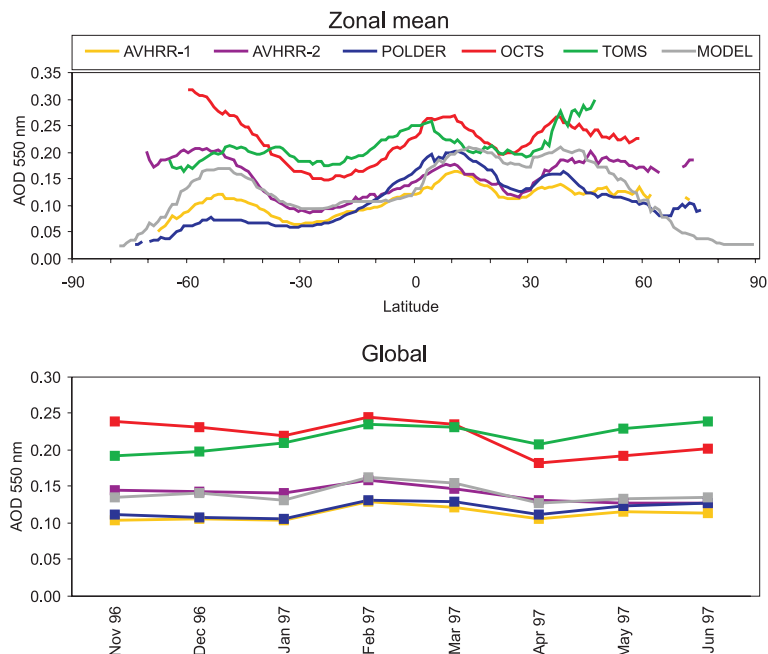

Fig. 4. Monthly mean AODs over ocean for 11 near coastal regions. Note the different *y*-axis for the Cape Verde Plateau. Regions defined in Myhre et al. (2005).

Fig. 5. Correlation on grid square level between model results and AVHRR-1, AVHRR-2, POLDER, OCTS, and TOMS for the 11 regions. Monthly mean data are used in the analysis.

A spatial correlation based between the modelled AOD and the satellite retrieval on the monthly data is shown in Fig. 5 for the 11 oceanic regions. This analysis is performed to investigate to which degree the modelled spatial pattern is similar to the satellite retrievals and to illustrate regional variations in the model–satellite comparison. The figure shows that the model has correlations around 0.6 to the AVHRR-1 and POLDER satellite retrievals for the 11 regions. Against the other satellite retrievals, the model has somewhat lower correlation which varies
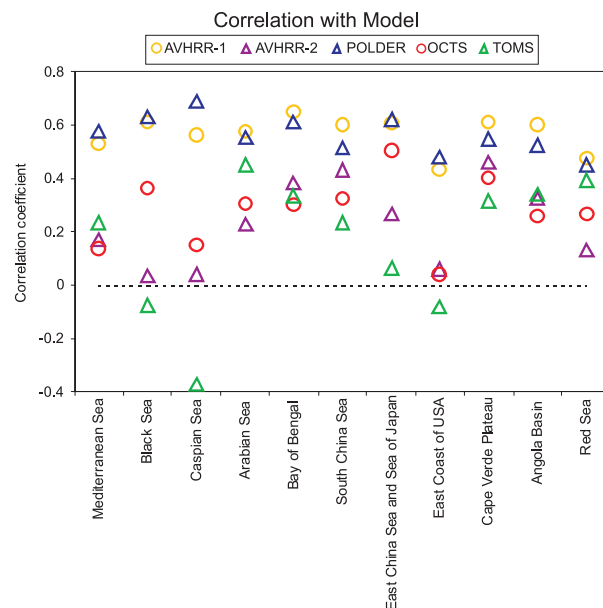
more between coastal regions than in the case of AVHRR-1 and POLDER.

4.3. Comparison with AERONET data

Figure 6 provides a comparison of monthly mean AOD between the model, satellite retrievals, and AERONET data.
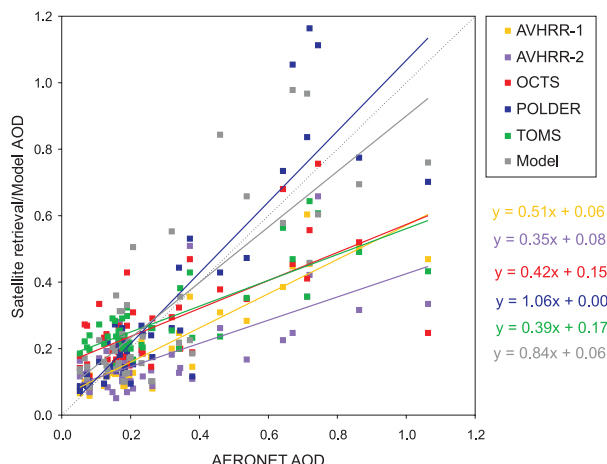
Fig. 6. Scatter plot of monthly mean AOD, the AERONET data versus each of the five satellite retrievals and the model results. Satellite data and model results at 550 nm, AERONET data mean of 440(500) and 670 nm.

Comparison with AERONET data is complicated and monthly mean data must be dealt with cautiously (Myhre et al., 2005). The spatial resolution, the number and time of the day of measurements, and cloud screening are different causes making such a comparison difficult. The model has a regression slope that is slightly below unity indicating a reasonable agreement with the AERONET data. The comparison between the satellite retrieval and AERONET is commented in Myhre et al. (2004a). The POLDER data compare best with AERONET data shown in Fig. 6. For the other satellite-retrieved data, the slope has a lower value, but note that the reduced slope is due to relatively few high AOD AERONET observations. Often these high AODs are from Cape Verde or Dakar. For Cape Verde a daily comparison for the year 1996 is performed in Grini et al. (2005). The main aerosol component at Cape Verde is mineral dust, and the model reproduces the main dust storms in 1996. The agreement was poorest for February and November of that year due to overestimation of two dust storms at this location.

4.4. Comparison of satellite and model derived radiative effect of aerosols

The POLDER and model-derived clear-sky aerosol direct radiative effect (RE) of aerosols is shown in Figs 7a and 7b as an eight-month average based on daily averaged numbers. The aerosol direct radiative effect is defined as the difference between radiative fluxes at the top of the atmosphere when aerosols are included and excluded. The patterns of the aerosol direct radiative effect of the aerosols in the two panels are very similar. Negative values are found in all regions. In both cases, an RE stronger than $-20\,\mathrm{Wm^{-2}}$ is calculated off the west coast of North Africa. An even stronger RE (stronger than $-100\,\mathrm{m^{-2}}$) was found during daytime in a dust event during the SHADE campaign (Haywood

et al., 2003b; Myhre et al., 2003b). The radiative effect is strong in coastal areas, and somewhat stronger in the model than in the POLDER data. The model has a stronger radiative effect of the aerosols around $50°$ in the Southern Hemisphere than the POLDER data and it can be seen from Fig. 2 that AOD in this region differs substantially. In other remote oceanic regions, the radiative effect of the aerosols is relatively weak. To avoid that differences in the radiative effect of the aerosols arise from differences in the AODs, we show in Figs 7c and 7d a comparison of the normalized radiative effect (NRE) (radiative effect divided by the AOD). Scattering by particles is more efficient at high solar zenith angles (Haywood and Shine, 1997) and thus the almost non-absorbing aerosols at high latitudes explain the large gradient in NRE at high latitudes. The NRE has a larger latitudinal variation in the POLDER derived product than in the model. Significantly larger NRE is found in POLDER than in the model at high latitudes. The reason for the different magnitude of NRE at high latitudes is unclear, but potentially differences in size distributions influence the results. Off the coast of the Saharan desert most of the AOD is from mineral dust, as indicated in Fig. 1. South of the Equator in Africa the AOD is clearly dominated by biomass burning. However, in a relatively small boarder region there is a complex mixture of mineral dust and biomass burning aerosols. Off the coast of the Saharan desert, the NRE is somewhat weaker in the model than in POLDER, whereas southward of this the NRE values are very similar, indicating good accordance for biomass burning aerosols and slight difference for mineral dust.

Figures 7e and 7f show the atmospheric absorption by the aerosols (ABS) for the POLDER and model-derived estimates. Note that these estimates include aerosol absorption as well as increased gas absorption due to scattering of the aerosols. The agreement between POLDER and the model is very good. Over remote oceanic regions the global transport model has somewhat higher values, which is likely related to the higher AOD in these regions. Close to the Asian continent the POLDER derived atmospheric absorption is somewhat higher, whereas the global aerosol transport model has somewhat higher values off the coast of western Africa. For POLDER and the model, the normalized atmospheric absorption (NAB) due to aerosols is shown in Figs 7g and 7h, respectively. The agreement is very good in coastal areas but the normalized atmospheric absorption from the aerosols is somewhat higher in the model in remote oceanic regions. In the current version of the POLDER-derived radiative effect of aerosols, a sea salt single scattering albedo at 670 nm of 1.0 is used, whereas in the original data a value of 0.98 was assumed (Bellouin et al., 2003). With a sea salt single scattering albedo of 0.98 a significantly stronger normalized atmospheric absorption was found in the POLDER than in the model in remote oceanic regions, with typical values around 15 $\mathrm{Wm^{-2}}$. In the model some transported black carbon from fossil fuel and biomass burning as well as mineral dust make the single scattering albedo slightly lower than 1.0, but still much higher than
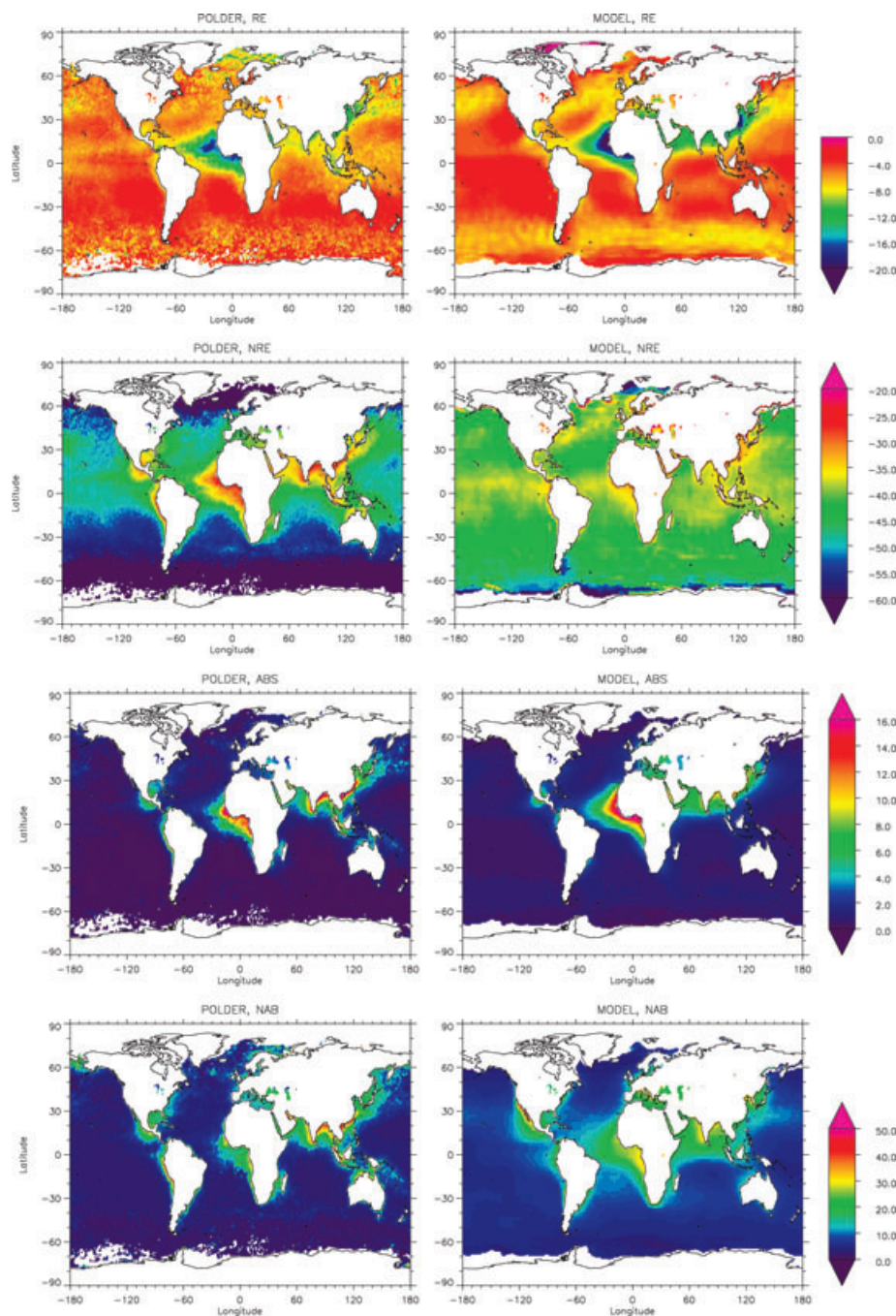
Fig. 7. Eight months average of RE, NRE, ABS and NAB for POLDER and Model for the period November 96–June 97. Values are in Wm^{-2}, but NRE and NAB is per unit AOD.

0.98 as used in the original POLDER data. The regions with high NAB in POLDER and the model are similar. Close to the Asian continent particularly high values are found in the Indian Ocean, a region with high content of black carbon from anthropogenic activity (Ramanathan et al., 2001b). Similar to what is illustrated here a large difference between the surface and top of the atmospheric radiative forcing has been shown earlier, with a potential

impact on the hydrological cycle (Ramanathan et al., 2001a; Ramanathan et al., 2001b; Kaufman et al., 2002). The NRE differs somewhat between POLDER and the model in the South East Asia coastal region. The RE is stronger in the model whereas the NRE is weaker than the POLDER data. The different result for RE and NRE arises from larger AOD in the model than in POLDER for this region (Fig. 2). Further, the slightly stronger
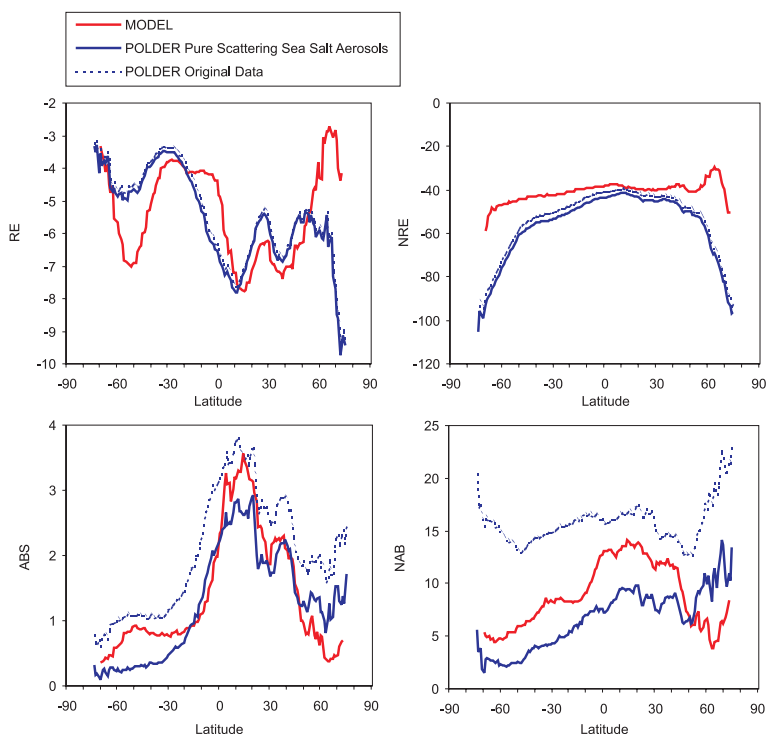
Fig. 8. Zonal average of RE, NRE, ABS and NAB for POLDER and Model for the period November 96–June 97 (all Wm^{-2}).

NAB in the POLDER data than in the model contributes to the differences for NRE in this region. West of Africa there is a high normalized atmospheric absorption mainly due to aerosols from biomass burning. Also around America (especially the central part) the high NAB values arise mainly from aerosols from biomass burning.

Fig. 8 shows the zonal mean of the quantities shown in Fig. 7. The radiative effect and atmospheric absorption of aerosols show good agreement, except at high northern latitudes. The difference at high northern latitudes in RE is mostly a result of disagreement in the NRE. For the atmospheric absorption from the aerosols it can be seen that the change in the single scattering albedo for sea salt from 0.98 to 1.0 is significant. The normalized radiative effect of the aerosols is weaker in the model than in the POLDER data, in particular at high latitudes. The zonal mean of the normalized atmospheric absorption of the aerosols from the model is mostly between the two POLDER data sets with different single scattering albedo for sea salt. The exception here is again at high latitudes.

Temporal variation in the normalized radiative effect and normalized atmospheric absorption of the aerosols is shown in Fig. 9 over large oceanic regions. For all cases, the temporal variation in the model follows quite nicely the POLDER data. As shown in Figs 7 and 8 the model has a weaker normalized radiative effect of the aerosols, and this is most pronounced in the Antarctic Ocean and least in the North Atlantic Ocean. For the normalized atmospheric absorption, the model results are between the

two POLDER data sets but mainly closest to the case with pure scattering sea salt aerosols.

Figures 10 and 11 show the temporal variation in the normalized radiative effect and normalized atmospheric absorption from the aerosols at several coastal areas. The model has weaker normalized radiative effect than the POLDER data, except at Cape Verde, the Arabian Sea, and the Bay of Bengal. It is only over the Black Sea and the Caspian Sea that the differences between the model and POLDER are significant, which may arise from assumption of the surface reflectance over these regions. Stronger aerosol absorption in the model cannot explain this difference since model calculations with purely scattering aerosols influence the results in these two areas by around 20%, which is similar to what is found in other regions. The normalized atmospheric absorption by the aerosols compares generally very well between the model and the POLDER data, including the temporal variations. The largest differences for this quantity are found at the Cape Verde Plateau and the Mediterranean Sea. Even in the Black Sea and the Caspian Sea the agreement is good, despite differences in the normalized radiative effect.

Table 3 shows the global mean numbers over oceans for the eight month period. Comparison with POLDER and the model is only possible for clear-sky condition. Simulations have been performed with the model neglecting radiative effect of aerosols in cloudy regions (cloud mask) and for including clouds (all sky). The cloud mask use the clear-sky RE, except when clouds
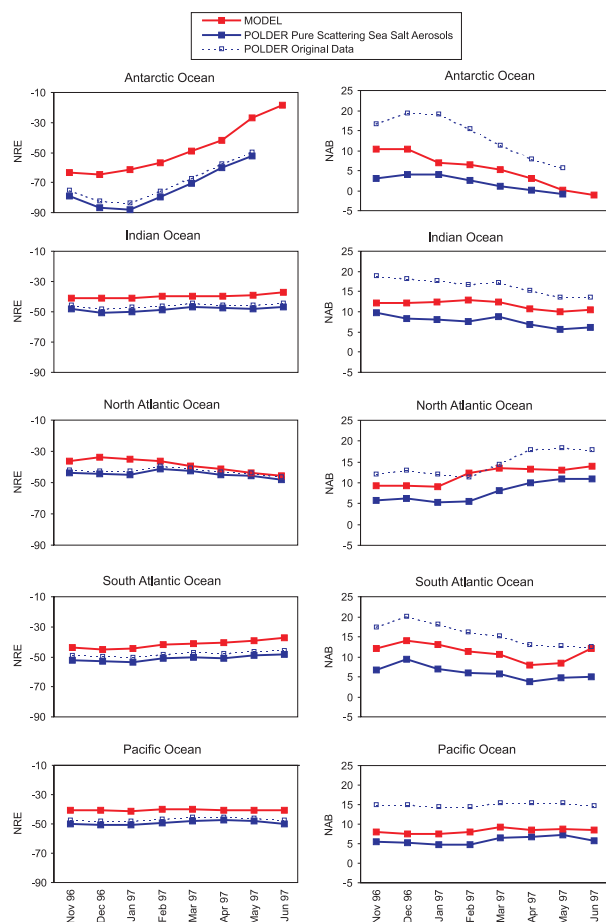
Fig. 9. Monthly average values of NRE and NAB (Wm^{-2}) from Model and POLDER for five oceanic regions for the time period November 96–June 97. Regions defined in Myhre et al. (2005).

5. Summary and discussion

A multicomponent global aerosol model has been compared to global oceanic data from five different satellite retrievals for an 8 month period in 1996 and 1997. Previous work has shown that these satellite data differ in retrieved AOD. The aerosol model estimates an AOD that is mostly within the range of the satellite retrievals. In comparison with AERONET data, the model also performs satisfactory. For one of the five satellite retrievals used in the AOD comparison, the direct aerosol radiative effect has been estimated previously. The radiative effect and atmospheric absorption is compared between the model and a data set derived based on POLDER retrievals. Similar patterns and magnitudes of the radiative effect and atmospheric absorption have been found. Somewhat larger differences were found when these quantities were normalized with AOD, in particular for the radiative effect at high latitudes. Our modelling results show a closer agreement with the satellite-derived radiative effect of aerosols compared to previously published model results. The five model estimates of RE in Yu et al. (2006) range between –4.7 and –1.6 Wm^{-2} and 10 out of the 11 satellite-derived estimates had stronger RE. The atmospheric absorption in the Oslo CTM2 is similar to the results from five models in Yu et al. (2006). Therefore, the AOD is higher or the NRE is stronger in Oslo CTM2 than in the other models. In any case Oslo CTM2 seems to yield results which are close to the available observations.

To gain confidence in calculations of radiative forcing of anthropogenic aerosols in global aerosol models, detailed comparison with available measurements is needed. Quantification of the absorbing aerosol is especially important since it has potential for changing the sign from a negative to a positive direct radiative forcing (Haywood and Shine, 1995; Jacobson, 2001; Myhre et al., 2003a; Sato et al., 2003). Further, absorbing aerosols may also be involved in a semidirect aerosol effect resulting in a global warming but local cooling (Menon et al., 2002). Menon et al. (2002) showed that absorbing aerosols in accordance with measurements of single scattering albedo could lead to a local cooling and changed precipitation pattern over China and India. This could explain observed trends in temperature and precipitation. Absorbing aerosols influence the solar energy more than scattering aerosols by increasing the atmospheric absorption significantly and also by reducing the solar radiation reaching the surface even more efficiently than scattering aerosols (Ramanathan et al., 2001a; Kaufman et al., 2002). The type of mixture between scattering and absorbing aerosols also influence the RE and atmospheric absorption. Several studies have shown that the single scattering albedo is significantly lower for an internal mixture than for an external mixture (e.g. Haywood and Shine, 1995). There is still a large uncertainty regarding the degree of mixing as well as type of mixing between various aerosols (Fuller et al., 1999; Mishchenko et al., 2004; Liu and Mishchenko, 2005). In our model, the RE and atmospheric absorption would be weakened and strengthened, respectively, by

are present then a zero RE are assumed. Simulations with the cloud mask are not performed intended to be realistic, but to gain insight how clouds impact the RE. Further, analysis with satellite-derived products can in some instances use the cloud mask RE approach. In the all sky simulation the contribution to RE comes from both clear sky and the cloudy sky. The cloud mask weakens the radiative effect of the aerosols significantly whereas the all sky radiative effect strengthens the radiative effect of the aerosols compared to the cloud mask. The latter result indicates that most of the absorbing aerosols above clouds do not play a major role in the model simulations; in such a case, the effect of including clouds would have been to give a positive radiative effect. The direct radiative effect of the aerosols at the top of the atmosphere for the time period studied here is similar to the mean of the remote sensed data found in Yu et al. (2006) for yearly averaged data. The atmospheric absorption in the atmosphere is weaker than what is found based on the remote sensed data.
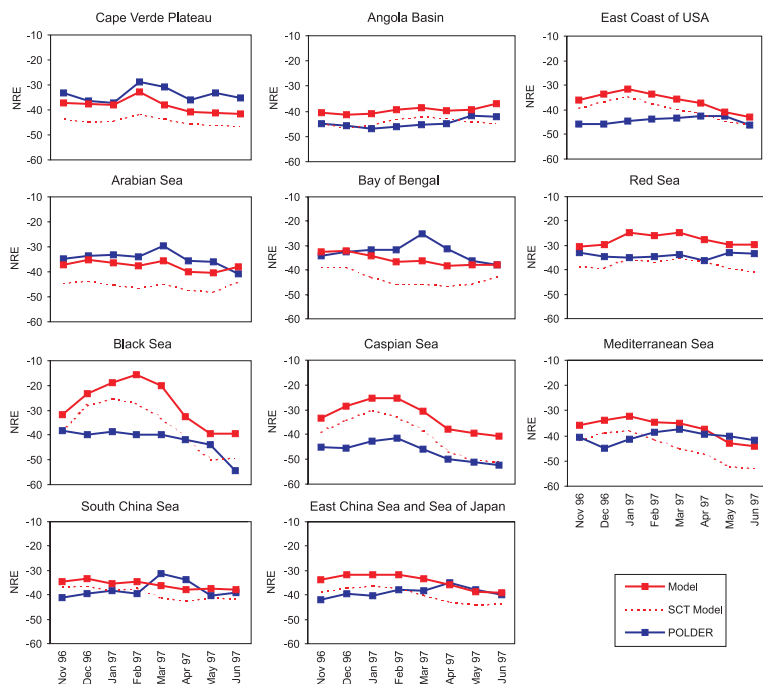
Fig. 10. Monthly average NRE (Wm^{-2}) from Model and POLDER for eleven oceanic subregions for the time period November 96–June 97. Model simulations have been performed assuming that the aerosols are pure scattering (SCT model). Regions defined in Myhre et al. (2005).
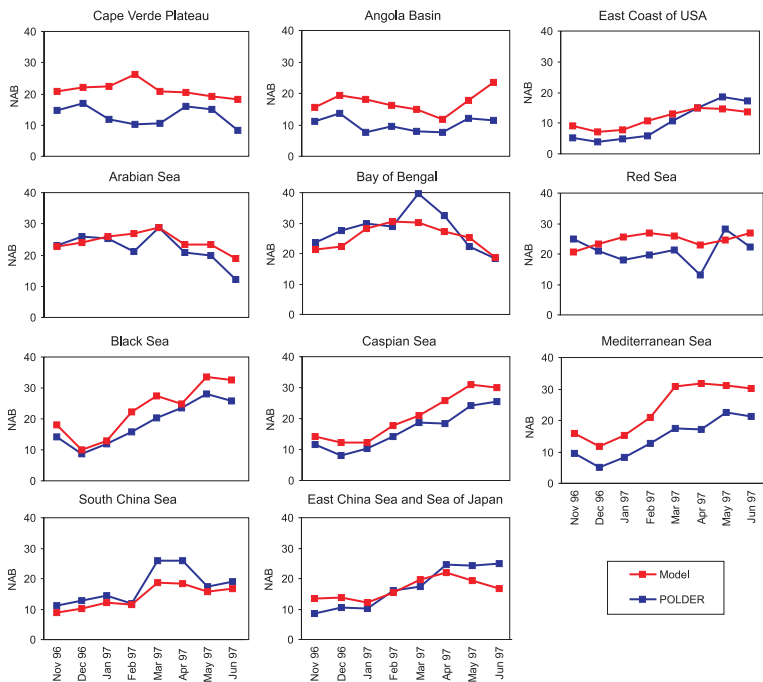

Fig. 11. Monthly average NAB (Wm^{-2}) from Model and POLDER for eleven oceanic subregions for the time period November 96–June 97.

assuming more internal mixing than assumption with external mixing. However, Mishchenko et al. (2004) found that semiexternal (aggregated particles) only modest change the single scattering albedo compared to external mixing. Based on the analysis made here, it is not possible to draw any firm conclusion regarding the assumption of external mixture. Internal mixing may also influence the hygroscopicity of the aerosols and thus the wet deposition.

In order to reduce the uncertainty related to the direct aerosol effect, one needs to improve knowledge on the optical and radiative properties as well as the aerosol concentrations and distributions. Substantial changes in the emissions of aerosols and their precursors have taken place during the last 1–2 decades (Vestreng and Støren, 2000; Carmichael et al., 2002; Novakov et al., 2003; Novakov and Hansen, 2004; Sharma et al., 2004). Improving these emission data, geographical distribution of the

Table 3. Global mean numbers over ocean of radiative effect and atmospheric absorption by the aerosols (Wm^{-2})

	POLDER	MODEL
Radiative effect at TOA clear sky	−5.6 (−52.7)	−5.5 (−40.2)
Atmospheric absorption by aerosols	1.4 (5.7)	1.5 (9.5)
Radiative effect at TOA cloud mask		−1.6
Radiative effect at TOA all sky		−2.3

The numbers in parentheses are normalized values for NRE and NAB.

emissions, and the trends are important for the modelling of many of the anthropogenic aerosols. In particular, improvements in the emissions of carbonaceous aerosols are needed, including year-to-year variations in biomass burning fires. Another aspect that needs to be investigated for the carbonaceous particles is the oxidation rates for these particles. Maria et al. (2004) indicated lower oxidation rates than previously recognized.

6. Acknowledgment

References

Abdou, W. A., Diner, D. J., Martonchik, J. V., Bruegge, C. J., Kahn, R. A. and co-authors. 2005. Comparison of coincident Multiangle Imaging Spectroradiometer and Moderate Resolution Imaging Spectroradiometer aerosol optical depths over land and ocean scenes containing Aerosol Robotic Network sites. *J. Geophys. Res.-Atmos.* **110**(D10), D10S07.

Ackerman, A. S., Toon, O. B., Stevens, D. E., Heymsfield, A. J., Ramanathan, V. and co-authors. 2000. Reduction of tropical cloudiness by soot. *Science* **288**(5468), 1042–1047.

Bellouin, N., Boucher, O., Haywood, J. and Reddy, M. S. 2005. Global estimate of aerosol direct radiative forcing from satellite measurements. *Nature* **438**, 1138–1141.

Bellouin, N., Boucher, O., Tanré, D. and Dubovik, O. 2003. Aerosol absorption over the clear-sky oceans deduced from POLDER-1 and AERONET observations. *Geophys. Res. Lett.* **30**(14), 1748.

Berglen, T. F., Berntsen, T. K., Isaksen, I. S. A. and Sundet, J. K. 2004. A global model of the coupled sulfur/oxidant chemistry in the troposphere: The sulfur cycle. *J. Geophys. Res.-Atmos.* **109**(D19), D19310.

Boucher, O. and Tanré, D. 2000. Estimation of the aerosol perturbation to the Earth's radiative budget over oceans using POLDER satellite aerosol retrievals. *Geophys. Res. Lett.* **27**(8), 1103–1106.

Carmichael, G. R., Streets, D. G., Calori, G., Amann, M., Jacobson, M. Z. and co-authors. 2002. Changing trends in sulfur emissions in Asia: Implications for acid deposition, air pollution, and climate. *Environ. Sci. Technol.* **36**(22), 4707–4713.

Christopher, S. A. and Zhang, J. L. 2002. Shortwave aerosol radiative forcing from MODIS and CERES observations over the oceans. *Geophys. Res. Lett.* **29**(18), 1859.

Cooke, W. F., Liousse, C., Cachier, H. and Feichter, J. 1999. Construction of a 1 degrees x 1 degrees fossil fuel emission data set for carbonaceous

aerosol and implementation and radiative impact in the ECHAM4 model. *J. Geophys. Res.-Atmos.* **104**(D18), 22137–22162.

Fitzgerald, J. W. 1975. Approximation Formulas For Equilibrium Size Of An Aerosol Particle As A Function Of Its Dry Size And Composition And Ambient Relative Humidity. *J. Appl. Meteorol.* **14**(6), 1044–1049.

Formenti, P., Elbert, W., Maenhaut, W., Haywood, J., Osborne, S. and co-authors. 2003. Inorganic and carbonaceous aerosols during the Southern African Regional Science Initiative (SAFARI 2000) experiment: Chemical characteristics, physical properties, and emission data for smoke from African biomass burning. *J. Geophys. Res.-Atmos.* **108**(D13), 8488.

Fuller, K. A., Malm, W. C. and Kreidenweis, S. M. 1999. Effects of mixing on extinction by carbonaceous particles. *J. Geophys. Res.-Atmos.* **104**(D13), 15941–15954.

Gauss, M., Isaksen, I. S. A., Wong, S. and Wang, W. C. 2003a. Impact of H2O emissions from cryoplanes and kerosene aircraft on the atmosphere. *J. Geophys. Res.-Atmos.* **108**(D10), 4304.

Gauss, M., Myhre, G., Pitari, G., Prather, M. J., Isaksen, I. S. A. and co-authors. 2003b. Radiative forcing in the 21st century due to ozone changes in the troposphere and the lower stratosphere. *J. Geophys. Res.-Atmos.* **108**(D9), 4292.

Ginoux, P., Chin, M., Tegen, I., Prospero, J. M., Holben, B. and co-authors. 2001. Sources and distributions of dust aerosols simulated with the GOCART model. *J. Geophys. Res.-Atmos.* **106**(D17), 20255–20273.

Goloub, P., Tanré, D., Deuze, J. L., Herman, M., Marchand, A. and co-authors. 1999. Validation of the first algorithm applied for deriving the aerosol properties over the ocean using the POLDER ADEOS measurements. *Ieee Trans. Geosci. Remote Sens.* **37**(3), 1586–1596.

Grini, A., Myhre, G., Sundet, J. K. and Isaksen, I. S. A. 2002. Modeling the annual cycle of sea salt in the global 3D model Oslo CTM2: Concentrations, fluxes, and radiative impact. *J. Clim.* **15**(13), 1717–1730.

Grini, A., Myhre, G., Zender, C. S. and Isaksen, I. S. A. 2005. Model simulations of dust sources and transport in the global atmosphere: Effects of soil erodibility and wind speed variability. *J. Geophys. Res.-Atmos.* **110**(D2), D02205.

Hansen, J., Sato, M. and Ruedy, R. 1997. Radiative forcing and climate response. *J. Geophys. Res.-Atmos.* **102**(D6), 6831–6864.

Haywood, J. and Boucher, O. 2000. Estimates of the direct and indirect radiative forcing due to tropospheric aerosols: A review. *Rev. Geophys.* **38**(4), 513–543.

Haywood, J., Francis, P., Osborne, S., Glew, M., Loeb, N. and co-authors. 2003b. Radiative properties and direct radiative effect of Saharan dust measured by the C-130 aircraft during SHADE: 1. Solar spectrum. *J. Geophys. Res.-Atmos.* **108**(D18), 8577.

Haywood, J. M., Osborne, S., Francis, P. N., Keil, A., Formenti, P. and co-authors. 2003a. The mean physical and optical properties of regional haze dominated by biomass burning aerosol measured from the C-130 aircraft during SAFARI 2000. *J. Geophys. Res.-Atmos.* **108**(D13), 8473.

Haywood, J. M., Ramaswamy, V. and Soden, B. J. 1999. Tropospheric aerosol climate forcing in clear-sky satellite observations over the oceans. *Science* **283**(5406), 1299–1303.

Haywood, J. M. and Shine, K. P. 1995. The Effect Of Anthropogenic Sulfate And Soot Aerosol On The Clear-Sky Planetary Radiation Budget. *Geophys. Res. Lett.* **22**(5), 603–606.

Haywood, J. M. and Shine, K. P. 1997. Multi-spectral calculations of the direct radiative forcing of tropospheric sulphate and soot aerosols using a column model. *Q. J. R. Meteorol. Soc.* **123**(543), 1907–1930.

Holben, B. N., Eck, T. F., Slutsker, I., Tanré, D., Buis, J. P. and co-authors. 1998. AERONET - A federated instrument network and data archive for aerosol characterization. *Remote Sens. Environ.* **66**(1), 1–16.

Holtslag, A. A. M., Debruijn, E. I. F. and Pan, H. L. 1990. A High-Resolution Air-Mass Transformation Model For Short-Range Weather Forecasting. *Mon. Weather Rev.* **118**(8), 1561–1575.

Houghton, J. T., and co-authors (eds), 2001. Climate Change 2001: The Scientific Basis. *Contribution of Working Group I to the Third Assessment Report of the Intergovernmental Panel on Climate Change.* Cambridge Univ. Press, UK/USA.

Husar, R. B., Prospero, J. M. and Stowe, L. L. 1997. Characterization of tropospheric aerosols over the oceans with the NOAA advanced very high resolution radiometer optical thickness operational product. *J. Geophys. Res.-Atmos.* **102**(D14), 16889–16909.

Isaksen, I. S. A., Zerefos, C., Kourtidis, K., Meleti, C., Dalsøren, S. and co-authors. 2005. Tropospheric ozone changes at unpolluted and semipolluted regions induced by stratospheric ozone changes. *J. Geophys. Res.-Atmos.* **110**(D2), D02302.

Jacobson, M. Z. 1999. Isolating nitrated and aromatic aerosols and nitrated aromatic gases as sources of ultraviolet light absorption. *J. Geophys. Res.-Atmos.* **104**(D3), 3527–3542.

Jacobson, M. Z. 2001. Strong radiative heating due to the mixing state of black carbon in atmospheric aerosols. *Nature* **409**(6821), 695–697.

Justus, C. G., Hargraves, W. R., Mikhail, A. and Graber, D. 1978. Methods For Estimating Wind Speed Frequency-Distributions. *J. Appl. Meteorol.* **17**(3), 350–353.

Kahn, R. A., Gaitley, B. J., Martonchik, J. V., Diner, D. J., Crean, K. A. and co-authors. 2005. Multiangle Imaging Spectroradiometer (MISR) global aerosol optical depth validation based on 2 years of coincident Aerosol Robotic Network (AERONET) observations. *J. Geophys. Res.-Atmos.* **110**(D10), D10S04.

Kaufman, Y. J., Boucher, O., Tanré, D., Chin, M., Remer, L. A. and co-authors. 2005. Aerosol anthropogenic component estimated from satellite data. *Geophys. Res. Lett.* **32**(17), L17804.

Kaufman, Y. J. and Fraser, R. S. 1997. The effect of smoke particles on clouds and climate forcing. *Science* **277**(5332), 1636–1639.

Kaufman, Y. J., Tanré, D. and Boucher, O. 2002. A satellite view of aerosols in the climate system. *Nature* **419**(6903), 215–223.

Kuang, Z. M. and Yung, Y. L. 2000. Reflectivity variations off the Peru Coast: Evidence for indirect effect of anthropogenic sulfate aerosols on clouds. *Geophys. Res. Lett.* **27**(16), 2501–2504.

Liu, L. and Mishchenko, M. I. 2005. Effects of aggregation on scattering and radiative properties of soot aerosols. *J. Geophys. Res.-Atmos.* **110**(D11), D11211.

Loeb, N. G. and Kato, S. 2002. Top-of-atmosphere direct radiative effect of aerosols over the tropical oceans from the Clouds and the Earth's Radiant Energy System (CERES) satellite instrument. *J. Clim.* **15**(12), 1474–1484.

Maria, S. F., Russell, L. M., Gilles, M. K. and Myneni, S. C. B. 2004. Organic aerosol growth mechanisms and their climate-forcing implications. *Science* **306**(5703), 1921–1924.

Menon, S., Hansen, J., Nazarenko, L. and Luo, Y. F. 2002. Climate effects of black carbon aerosols in China and India. *Science* **297**(5590), 2250–2253.

Mishchenko, M. I., Geogdzhayev, I. V., Cairns, B., Rossow, W. B. and

Lacis, A. A. 1999. Aerosol retrievals over the ocean by use of channels 1 and 2 AVHRR data: sensitivity analysis and preliminary results. *Appl. Opt.* **38**(36), 7325–7341.

Mishchenko, M. I., Geogdzhayev, I. V., Liu, L., Ogren, J. A., Lacis, A. A. and co-authors. 2003. Aerosol retrievals from AVHRR radiances: effects of particle nonsphericity and absorption and an updated long-term global climatology of aerosol properties. *J.l Quant. Spectrosc. Radiat. Transfer* **79/80**, 953–972.

Mishchenko, M. I., Lacis, A. A., Carlson, B. E. and Travis, L. D. 1995. Nonsphericity Of Dust-Like Tropospheric Aerosols - Implications For Aerosol Remote-Sensing And Climate Modeling. *Geophys. Res. Lett.* **22**(9), 1077–1080.

Mishchenko, M. I., Liu, L., Travis, L. D. and Lacis, A. A. 2004. Scattering and radiative properties of semi-external versus external mixtures of different aerosol types. *J. Quant. Spectrosc. Radiat. Transfer* **88**(1-3), 139–147.

Monahan, E., Spiel, D. and Spiel, K. 1986. *Oceanic whitecaps.* Reidel.

Myhre, C. E. L. and Nielsen, C. J. 2004. Optical properties in the UV and visible spectral region of organic acids relevant to tropospheric aerosols. *Atmos. Chem. Phys.* **4**, 1759–1769.

Myhre, G., Berglen, T. F., Myhre, C. E. L. and Isaksen, I. S. A. 2004b. The radiative effect of the anthropogenic influence on the stratospheric sulfate aerosol layer. *Tellus* **56B**(3), 294–299.

Myhre, G., Berntsen, T. K., Haywood, J. M., Sundet, J. K., Holben, B. N. and co-authors. 2003a. Modeling the solar radiative impact of aerosols from biomass burning during the Southern African Regional Science Initiative (SAFARI-2000) experiment. *J. Geophys. Res.-Atmos.* **108**(D13), 8501.

Myhre, G., Grini, A., Haywood, J. M., Stordal, F., Chatenet, B. and co-authors. 2003b. Modeling the radiative impact of mineral dust during the Saharan Dust Experiment (SHADE) campaign. *J. Geophys. Res.-Atmos.* **108**(D18), 8579.

Myhre, G., Jonson, J. E., Bartnicki, J., Stordal, F. and Shine, K. P. 2002. Role of spatial and temporal variations in the computation of radiative forcing due to sulphate aerosols: A regional study. *Q. J. R. Meteorol. Soc.* **128**(581), 973–989.

Myhre, G., Stordal, F., Berglen, T. F., Sundet, J. K. and Isaksen, I. S. A. 2004c. Uncertainties in the radiative forcing due to sulfate aerosols. *J. Atmos. Sci.* **61**(5), 485–498.

Myhre, G., Stordal, F., Johnsrud, M., Diner, D. J., Geogdzhayev, I. V. and co-authors. 2005. Intercomparison of satellite retrieved aerosol optical depth over ocean during the period September 1997 to December 2000. *Atmos. Chem. Phys.* **5**, 1697–1719.

Myhre, G., Stordal, F., Johnsrud, M., Ignatov, A., Mishchenko, M. I. and co-authors. 2004a. Intercomparison of satellite retrieved aerosol optical depth over the ocean. *J. Atmos. Sci.* **61**(5), 499–513.

Nakajima, T. and Higurashi, A. 1998. A use of two-channel radiances for an aerosol characterization from space. *Geophys. Res. Lett.* **25**(20), 3815–3818.

Nakajima, T., Higurashi, A., Kawamoto, K. and Penner, J. E. 2001. A possible correlation between satellite-derived cloud and aerosol microphysical parameters. *Geophys. Res. Lett.* **28**(7), 1171–1174.

Novakov, T. and Hansen, J. E. 2004. Black carbon emissions in the United Kingdom during the past four decades: an empirical analysis. *Atmos. Environ.* **38**(25), 4155–4163.

Novakov, T., Ramanathan, V., Hansen, J. E., Kirchstetter, T. W., Sato, M. and co-authors. 2003. Large historical changes of fossil-fuel black carbon aerosols. *Geophys. Res. Lett.* **30**(6), 1324.

Peng, C., Chan, M. N. and Chan, C. K. 2001. The hygroscopic properties of dicarboxylic and multifunctional acids: Measurements and UNIFAC predictions. *Environ.l Sci. Technol.* **35**(22), 4495–4501.

Prather, M. J. 1986. Numerical Advection By Conservation Of 2nd-Order Moments. *J. Geophys. Res.-Atmos.* **91**(D6), 6671–6681.

Ramanathan, V., Crutzen, P. J., Kiehl, J. T. and Rosenfeld, D. 2001a. Atmosphere - Aerosols, climate, and the hydrological cycle. *Science* **294**(5549), 2119–2124.

Ramanathan, V., Crutzen, P. J., Lelieveld, J., Mitra, A. P., Althausen, D. and co-authors. 2001b. Indian Ocean Experiment: An integrated analysis of the climate forcing and effects of the great Indo-Asian haze. *J. Geophys. Res.-Atmos.* **106**(D22), 28371–28398.

Remer, L. A., Kaufman, Y. J., Tanré, D., Mattoo, S., Chu, D. A. and co-authors. 2005. The MODIS aerosol algorithm, products, and validation. *J. Atmos. Sci.* **62**(4), 947–973.

Rosenfeld, D., Lahav, R., Khain, A. and Pinsky, M. 2002. The role of sea spray in cleansing air pollution over ocean via cloud processes. *Science* **297**(5587), 1667–1670.

Sato, M., Hansen, J., Koch, D., Lacis, A., Ruedy, R. and co-authors. 2003. Global atmospheric black carbon inferred from AERONET. *Proc. Natl. Acad. Sci. USA* **100**(11), 6319–6324.

Seinfeld, J. H. and Pandis, S. N. 1998. *Atmospheric chemistry and physics, From air pollution to Climate change*. John Wiley and Sons, New York.

Sekiguchi, M., Nakajima, T., Suzuki, K., Kawamoto, K., Higurashi, A. and co-authors. 2003. A study of the direct and indirect effects of aerosols using global satellite data sets of aerosol and cloud parameters. *J. Geophys. Res.-Atmos.* **108**(D22), 4699.

Sharma, S., Lavoue, D., Cachier, H., Barrie, L. A. and Gong, S. L. 2004. Long-term trends of the black carbon concentrations in the Canadian Arctic. *J. Geophys. Res.-Atmos.* **109**(D15), D15203.

Shettle, E. and Fenn, R. 1979. Models for the aerosols of the lower atmosphere and the effects of humidity variations on their optical properties. Tech. Rep. TR-79-0214.

Smith, M. H., Park, P. M. and Consterdine, I. E. 1993. Marine Aerosol Concentrations And Estimated Fluxes Over The Sea. *Q. J. R. Meteorol. Soc.* **119**(512), 809–824.

Stamnes, K., Tsay, S. C., Wiscombe, W. and Jayaweera, K. 1988. Numerically Stable Algorithm For Discrete-Ordinate-Method Radiative-Transfer In Multiple-Scattering And Emitting Layered Media. *Appl. Opt.* **27**(12), 2502–2509.

Stowe, L. L., Ignatov, A. M. and Singh, R. R. 1997. Development, validation, and potential enhancements to the second-generation operational aerosol product at the national environmental satellite, data, and information service of the national oceanic and atmospheric administration. *J. Geophys. Res.-Atmos.* **102**(D14), 16923–16934.

Tanré, D., Breon, F. M., Deuze, J. L., Herman, M., Goloub, P. and co-authors. 2001. Global observation of anthropogenic aerosols from satellite. *Geophys. Res. Lett.* **28**(24), 4555–4558.

Tiedtke, M. 1989. A Comprehensive Mass Flux Scheme For Cumulus Parameterization In Large-Scale Models. *Mon. Weather Rev.* **117**(8), 1779–1800.

Toon, O. B., Pollack, J. B. and Khare, B. N. 1976. Optical-Constants Of Several Atmospheric Aerosol Species - Ammonium-Sulfate, Aluminum-Oxide, And Sodium-Chloride. *J. Geophys. Res.-Oceans and Atmos.* **81**(33), 5733–5748.

Torres, O., Bhartia, P. K., Herman, J. R., Ahmad, Z. and Gleason, J. 1998. Derivation of aerosol properties from satellite measurements of backscattered ultraviolet radiation: Theoretical basis. *J. Geophys. Res.-Atmos.* **103**(D14), 17099–17110.

Vestreng, V. and Støren, E. 2000. Analysis of UNEP/EMEP Emission Data. EMEP/MSC-W Note 1/00.

WCP, N. Y. 1986. A preliminary cloudless standard atmosphere. Rep. WCP-112.

Wetzel, M. A. and Stowe, L. L. 1999. Satellite-observed patterns in stratus microphysics, aerosol optical thickness, and shortwave radiative forcing. *J. Geophys. Res.-Atmos.* **104**(D24), 31287–31299.

Yu, H., Kaufman, Y. J., Chin, M., Feingold, G., Remer, L. A. and co-authors. 2006. A review of measurement-based assessments of the aerosol direct radiative effect and forcing. *Atmos. Chem. Phys.* **6**, 613–666.

Zender, C. S., Bian, H. S. and Newman, D. 2003. Mineral Dust Entrainment and Deposition (DEAD) model: Description and 1990s dust climatology. *J. Geophys. Res.-Atmos.* **108**(D14), 4416.

Zhang, J. L., Christopher, S. A., Remer, L. A. and Kaufman, Y. J. 2005. Shortwave aerosol radiative forcing over cloud-free oceans from Terra: 2. Seasonal and global distributions. *J. Geophys. Res.-Atmos.* **110**(D10), D10S24.